Efficient Partial Volume Tissue Classification in MRI Scans

Aljaž Noe[1] and James C. Gee[2]

[1] Faculty of Electrical Engineering, University of Ljubljana
[2] Department of Radiology, University of Pennsylvania

Abstract. A probabilistic tissue classification algorithm is described for robust MR brain image segmentation in the presence of partial volume averaging. Our algorithm estimates the fractions of all tissue classes present in every voxel of an image. In this work, we discretize the fractional content of tissues in *partial volume voxels*, to obtain a finite number of mixtures. Every mixture has a label assigned to it, and the algorithm searches for the labeling that maximizes the posterior probability of the labeled image. A prior is defined to favor spatially continuous regions while taking into an account different tissue mixtures. We show that this extension of an existing partial volume clustering algorithm, [8], improves the quality of segmentation, without increasing the complexity of the procedure. The final result is the estimated fractional amount of each tissue type present within a voxel in addition to the label assigned to the voxel.

1 Introduction

In this work, we consider the problem of segmenting magnetic resonance (MR) images, which is made difficult by the existence of partial volume (PV) averaging and intensity shading artifacts due to limited spatial resolution of the scanner and RF field inhomogeneity, respectively. To improve the quantitative precision of segmentation, we develop a method for determining the fractional content of each tissue class for so-called partial volume voxels of mixed tissue type, taking into account shading artifacts. Of specific interest in the current work are the primary tissue constituents of the brain: gray (GM) and white matter (WM) as well as cerebrospinal fluid (CSF).

Two general approaches have been applied to address the problem of partial volume (PV) segmentation. In [2,7], a *mixel model*, assumes that every voxel in an image is a PV voxel, consisting of a mixture of pure tissue classes. Because of the number of parameters that must be estimated, either multi-channel data and/or additional constraints are required to obtain the segmentation solution. A second approach, [8,5,9] to dealing with PV voxels is to marginalize over the variables describing the fractional portions of each *pure tissue class*. This produces an additional, new set of *partial volume classes*, with which each image voxel may be associated. However, an additional estimation step is necessary to obtain the fractional amount of different tissues in each voxel.

T. Dohi and R. Kikinis (Eds.): MICCAI 2002, LNCS 2488, pp. 698–705, 2002.

In the current work we develop a method that shares aspects of both approaches. In the mixel-model approach, noise in the image limits the precision with which the fractional tissue content in PV voxels can be estimated from the image. This in turn results in either a noisy or over smoothed final segmentation. The marginalization approach identifies PV voxels, but does not provide an estimate of the tissue fractions for these voxels. Moreover, both approaches are computationally expensive. The mixel model entails a large number on unknowns, whereas the marginalization requires numeric integration to obtain a distribution function of PV classes.

We propose to use only a *finite* number of mixtures for a given pair of tissue classes to model the PV averaging effect. In this way, marginalization is not required and the fractional tissue content of PV voxels is directly provided by the mixture label. The precision of the fractional tissue estimates can be controlled through the appropriate discretization of the continuous mixture.

While this approach can and should also be used within the implementation of the clustering procedure for the estimation of class probability parameters, we choose to treat it separately to be able to obtain unbiased evaluation of its functionality.

2 Image Model

Let $\mathbf{y}_i = (y_{i,1}, y_{i,2}, \dots y_{i,M})^T$ be the M-channel observation at the i-th voxel of an input image. At each voxel we assume there exists a mixture of several different tissue types. The contribution of a specific tissue type to the voxel measurement is weighted by its fractional ammount in the voxel. Tissues are modeled by voxel classes that are assumed to have Gaussian probability distribution of the intensity. This type of image model was also used by several other authors [2,7] and in part also by [5,9]. Measurement at each voxel is modeled as a linear combination of Gaussian random variables:

$$\mathbf{y}_i = \sum_{k \in \mathcal{K}} t_{i,k} \mathbf{N}(\boldsymbol{\mu}_k(i), \boldsymbol{\Sigma}_k)\,, \quad \sum_{k \in \mathcal{K}} t_{i,k} = 1\,, \quad 0 \le t_{i,k} \le 1\,, \tag{1}$$

where $\mathbf{N}(\boldsymbol{\mu}_k, \boldsymbol{\Sigma}_k)$ represents a multivariate Gaussian random variable with $\boldsymbol{\mu}_k = (\mu_{k,1}, \dots, \mu_{k,M})^T$ the vector of mean intensity values (M channels), and $\boldsymbol{\Sigma}_k$ is the associated M-by-M covariance matrix for the M-channel observation. Each tissue class k can have different mean and variance, where $\mathcal{K}$ is the set of permissible tissue types. Note that mean vector $\boldsymbol{\mu}_k(i)$ is also a function of voxel location i, which allows us to take into account intensity inhomogeneities that may be present in the data.

$t_{i,k}$ represents the fraction of pure tissue class k that is present at the i-th voxel. The goal of the partial volume segmentation is to estimate $t_{i,k}\,, \forall k \in \mathcal{K}$ for each voxel i in the image. In order to do that, we can solve (1) for each i. Since we have in general more than one unknown variable per equation and there is also noise present in an image, the problem is severely under constrained. Additional constraints must therefore be introduced on the image model.

In [6] the PV effect is assumed to be caused by downsampling a high resolution image. We use this idea and constrain the image model in (1) in two ways. First, we assume the number of different tissue types in a voxel is limited to two, which in practice introduces negligible error in the image model. Second, we discretize the continuous mixture variable and consider only a finite number of mixture possibilities:

$$\begin{aligned} t_{i,k} &\in \mathcal{T}\,, \\ \mathcal{T} &= \{\tau_1, \tau_2, \ldots, \tau_T\}\,, \quad \tau_i \neq \tau_j\,. \end{aligned} \tag{2}$$

The motivation for the latter constraint is that the presence of image noise may limit the precission with which the fractional tissue content can be estimated. This constraint, on the other hand, makes the problem of estimating fractions of pure tissue classes much easier.

In practical applications the number of specific mixtures T is chosen to obtain a compromise between the amount of partial volume voxels in the image, required precision of segmentation and the computational time. We then consider these mixtures as additional voxel classes in our image—*mixture classes*. Since the measurement of each mixture class is defined by a linear combination of two Gaussian random variables, the distribution of mixtures is again a Gaussian distribution, with the following mean and variance:

$$\begin{aligned} \boldsymbol{\mu}_{t,k_1,k_2} &= \boldsymbol{\mu}_{k_1} + (1-t)\boldsymbol{\mu}_{k_2} \\ \boldsymbol{\Sigma}_{t,k_1,k_2} &= t^2\boldsymbol{\Sigma}_{k_1} + (1-t)^2\boldsymbol{\Sigma}_{k_2}\,, \end{aligned} \tag{3}$$

where $t \in \mathcal{T}$ is the specific mixture ratio between tissue classes k_1 and k_2. When segmenting MR images of the brain, we define two sets of mixtures: one modeling PV voxels containing CSF and GM, and the other modeling the voxels containing GM and WM. A different label λ is assigned to every mixture class—one for each (t, k_1, k_2) triplet.

2.1 Bayesian Formulation of Segmentation Problem

The posterior probability of the classification $\boldsymbol{\Lambda}$ given the data $\mathbf{Y}$ is defined as:

$$P(\boldsymbol{\Lambda}|\mathbf{Y}) = \frac{P(\mathbf{Y}|\boldsymbol{\Lambda})P(\boldsymbol{\Lambda})}{P(\mathbf{Y})}\,, \tag{4}$$

where $P(\mathbf{Y}|\boldsymbol{\Lambda})$ is our observation/image model and $P(\boldsymbol{\Lambda})$ is a prior on the label field. As in [9], we use a Potts model for the prior to penalize the granualities in the labeling,

$$P(\boldsymbol{\Lambda}) = \frac{1}{Z}\exp\left[-\beta\sum_i\sum_{j\in\mathcal{N}_i}\delta\left(\lambda_i,\lambda_j\right)\right]\,, \tag{5}$$

where β is a constant that controls the strength of a prior, $\mathcal{N}_i$ is the set of voxels in some neighborhood of voxel i and Z is a scaling constant. $\delta\left(\lambda_i,\lambda_i\right)$ defines the "similarity" between mixture classes λ_i and λ_j. Specifically $\delta\left(\lambda_i,\lambda_j\right) = \frac{o}{d(i,j)}$,

Table 1. Tissue overlap between different mixture classes. First three columns/rows correspond to pure classes, and the rest are different PV mixtures—here we have 4 different PV mixture ratios. Column labels are identical to rows labels but are partially omited to save space. By changing the values in this table, different mixture classes can be favored.

mixture class	**CSF**	**GM**	**WM**	.	.	.	.	.	.	.	.
CSF	1.0	0.0	0.0	0.8	0.6	0.4	0.2	0.0	0.0	0.0	0.0
GM	0.0	1.0	0.0	0.2	0.4	0.6	0.8	0.8	0.6	0.4	0.2
WM	0.0	0.0	1.0	0.0	0.0	0.0	0.0	0.2	0.4	0.6	0.8
0.8CSF, 0.2GM	0.8	0.2	0.0	1.0	0.8	0.6	0.4	0.2	0.2	0.2	0.2
0.6CSF, 0.4GM	0.6	0.4	0.0	0.8	1.0	0.8	0.6	0.4	0.4	0.4	0.2
0.4CSF, 0.6GM	0.4	0.6	0.0	0.6	0.8	1.0	0.8	0.6	0.6	0.4	0.2
0.2CSF, 0.8GM	0.2	0.8	0.0	0.4	0.6	0.8	1.0	0.8	0.6	0.4	0.2
0.8GM, 0.2WM	0.0	0.8	0.2	0.2	0.4	0.6	0.8	1.0	0.8	0.6	0.4
0.6GM, 0.4WM	0.0	0.6	0.4	0.2	0.4	0.6	0.6	0.8	1.0	0.8	0.6
0.4GM, 0.6WM	0.0	0.4	0.6	0.2	0.4	0.4	0.4	0.6	0.8	1.0	0.8
0.2GM, 0.8WM	0.0	0.2	0.8	0.2	0.2	0.2	0.2	0.4	0.6	0.8	1.0

where $0 \leq o \leq 1$ is the amount of "tissue overlap" between the two mixture classes λ_i and λ_j and $d(i,j)$ is the distance between voxels i and j. Overlap values are shown in table 1. This definition favors smooth transition of estimated fractions between regions of pure tissue type.

We find the labeling $\mathbf{\Lambda}$ that maximizes the posterior probability $P(\mathbf{\Lambda}|\mathbf{Y})$:

$$\mathbf{\Lambda} = \arg\max_{\mathbf{\Lambda}} P(\mathbf{\Lambda}|\mathbf{Y})\,. \tag{6}$$

3 Implementation

We use the ICM algorithm [1] to maximize the posterior probability (4):

$$\lambda_i^{n+1} = \arg\max_{\lambda} \left[\log P(\mathbf{y}_i|\lambda) - \beta \sum_{j \in \mathcal{N}_i} \delta(\lambda, \lambda_j^n) \right], \tag{7}$$

where $P(\mathbf{y}_i|\lambda)$ is the conditional probability density function for observing $\mathbf{y}$ at voxel i given mixture class λ, and λ_i^n is the mixture label for voxel i computed at n-th iteration.

In order to evaluate $P(\mathbf{y}_i|\lambda)$, its parameters $\boldsymbol{\mu}_k$ and $\mathbf{\Sigma}_k$, must be estimated from the image prior to the classification. We use maximum likelihood mixture model clustering [8] to estimate these parameters externally without affecting the classifier. The expectation maximization algorithm is used to iteratively update the class parameters:

$$\boldsymbol{\mu}_k = \frac{\sum_{i=1}^N P(k|\mathbf{y}_i) \cdot \mathbf{y}_i}{h_k}\,; \qquad \mathbf{\Sigma}_k = \frac{\sum_{i=1}^N P(k|\mathbf{y}_i) \cdot \mathbf{y_i} \cdot \mathbf{y}_i^T}{h_k} - \boldsymbol{\mu}_k \cdot \boldsymbol{\mu}_k^T\,; \tag{8}$$
$$h_k = \textstyle\sum_{i=1}^N P(k|\mathbf{y}_i)\,, \quad k \in \mathcal{K}\,.$$

The clustering algorithm also takes into account any PV averaging that may be present in the image and in addition estimates the intensity nonuniformity field, thus obtaining the class mean intensity value for each voxel in the image $\boldsymbol{\mu}_k(i)$. This implies that probability density functions $P(\mathbf{y}_i|k)$ are also spatially dependent. The mean values and variances of a specific mixture class can then be computed for any i using (3).

4 Experiments and Discussion

In order to evaluate the segmentation accuracy of the proposed method we require a test image for which a ground truth partial volume information is available. Manual segmentations of real MR data do not provide such information. We must therefore resort to the use of simulated MR images. Specifically we used the 1 mm T1, BrainWeb[3,4] phantom images produced by the McConnell Brain Imaging Centre at the Montreal Neurological Institute. For each simulated image, true fraction of the gray and white matter and cerebrospinal fluid is known at every voxel in an image. Parameter β was set to 0.4 and 4 ICM iterations were used.

To estimate the disparity between the segmentation results and ground truth, we calculated the mean squared difference between the estimated and true fractional values over the entire image for each tissue type. Images with various amounts of noise were segmented into 3 pure tissue classes (GM, WM, CSF) and 2 PV classes (GM/WM, GM/CSF) with 9 different mixtures each. This gives a total of 21 different classes into which each image voxel can be segmented. The mean square differences averaged over all tissue types were 0.0182, 0.0086 and 0.0048 for BrainWeb images containing 9%, 3% and 0% noise respectively. Results of the evaluation are presented in Fig. 1.

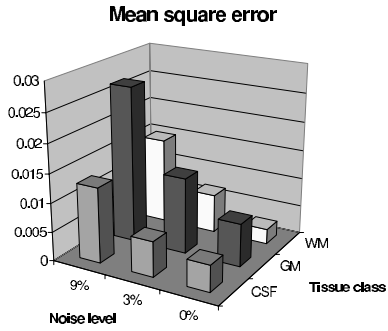

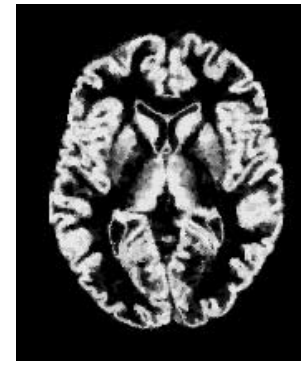

Fig. 1. Segmentation results for BrainWeb phantom. (Left) Mean square error in estimation of tissue fractions. (Right): Example gray matter segmentation.

We found slight difference between the current results of our BrainWeb segmentation and those obtained using a marginalization approach [8] in favor of the former. This is in part due to relatively small amount of partial volume artifact present in the data. Although the spatial prior reduces noise in the segmented image, it also introduces smoothing, which is manifested as errors in segmentation.

Since the number of partial volume voxels is small in comparison to the size of the BrainWeb image, changing the number of mixture classes has little effect on the segmentation results. To further explore the relationship between the amount of noise in the image, number of mixture classes and the quality of segmentation, we performed a series of tests on a synthetic images of a square, exhibiting different amounts of noise and partial volume averaging artifact.

We constructed a square, 300-by-300, image and subdivided the image into 3 regions, each separated by a vertical boundary. The left and right most regions were considered pure "tissues" and their image values were drawn from normal distributions with the following mean and variance values, respectively: $\mu_1 = 70$, $\Sigma_1 = 100$ and $\mu_2 = 150$, $\Sigma_2 = 400$. The middle strip of the image, 100 pixels wide, contained partial volume pixels, which modeled a smooth linear transition between the two pure classes. The synthetic image is shown in Fig. 2.

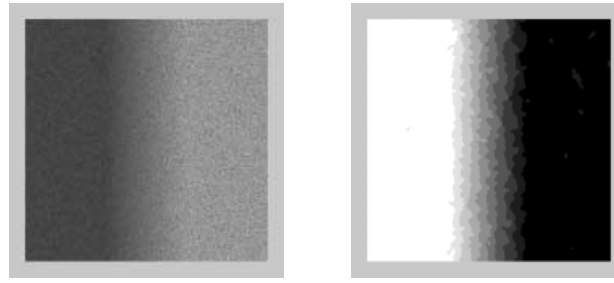

Fig. 2. Synthetic data. (Left) Test image used in evaluation. (Right) Segmentation result for using 8 PV mixtures, where the intensity reflects the fractional content—white indicates 100%, black 0%.

In Fig. 3, we show the mean square error in segmentation as a function of the number of mixtures. We can clearly observe the inverse relationship between these two parameters. We can see that increasing the number of mixture classes beyond a certain number only minimally improves the segmentation. This enables considerable savings in computational time compared to the marginalization approach for PV segmentation, by avoiding numerical integration required to obtain PV distribution. This holds for both the clustering step, where class parameters are estimated, as well as during the voxel classification procedure. We have also observed that the number of steps required for the ICM algorithm to converge increases with the number of mixture classes. It however remains manageble, and we never had to use more than 15 steps to achieve convergence.

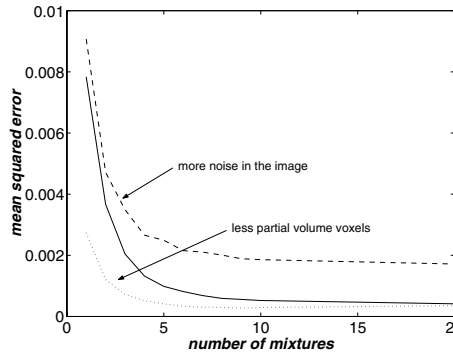

Fig. 3. Relationship between the mean square error in segmentation of the synthetic image of a square and number of PV mixture classes used in the segmentation. Solid line shows the error for image as defined above, dashed line represents error for the image that contained three times the amount of noise and dotted line is for the image that contained only one third of the partial volume effect.

We observed minimal changes in the above relationship as a result of different noise levels in the image. The difference in image noise is directly related to the segmentation error and does not affect the ratio between number of mixtures and error. The amount of PV voxels in the image, however, clearly affects this ratio and thereby defines the optimal number of mixtures. This allows us to efficiently segment images with various amounts of PV averaging, by simply changing the number of mixture classes accordingly.

Although this is not clearly visible in the graph, we have also observed a slight increase in error when number of mixture classes was too large. Error when using 20 mixture classes was for example larger than it was when only 10 mixtures were used. While this error could be contributed to the fact that the ICM algorithem simply did not finish in the minimum, there nevertheless clearly exists a number of mixture classes, that provides an optimal balance between segmentation error and numeric complexity.

5 Summary

We presented a method for partial volume segmentation of MR images. The method represents an intermediate approach between the estimation of continuous tissue fractions in the image model (1) and the addition of a single class with which all partial volume voxels of a certain tissue combination are labeled regardless of the mixture ratio of the combination. The modeling of multiple mixture ratios in the current work enables a more efficient implementation than the latter approach in which a marginalization must be numerically evaluated. Furthermore, our method's small number of unknown parameters in comparison to mixel model based-methods results in a more stable algorithms. At the same time, in preliminary evaluations, we found little degradation in partial volume

segmentation accuracy as a consequence of using only a discrete range of mixture ratios. This remains to be validated on a more comprehensive data set, which is planned for the future.

References

1. Julian Besag. On the Statistical Analysis of Dirty Pictures. *Journal of the Royal Statistical Society, Series B*, 48(3):259–302, 1986.
2. Hwan Soo Choi, David R. Haynor, and Yongmin Kim. Partial volume tissue classification of multichannel magnetic resonance images - a mixel model. *IEEE Transactions on Medical Imaging*, 10(3):395–407, September 1991.
3. `http://www.bic.mni.mcgill.ca/brainweb/`.
4. R.K.-S. Kwan, A.C. Evans, and G. B. Pike. *An Extensible MRI Simulator for Post-Processing Evaluation*, volume 1131 of *Lecture Notes in Computer Science*, pages 135–140. Springer-Verlag, May 1996.
5. David H. Laidlaw, Kurt W. Flescher, and Alan H. Barr. Partial-volume bayesian classification of material mixtures in MR volume data using voxel histograms. *IEEE Transactions on Medical Imaging*, 17(1):74–86, February 1998.
6. Koen Van Leemput and Paul Suetens Frederik Maes, Dirk Vandermeulen. A statistical framework for partial volume segmentation. In *Proceedings 4th international conference on medical image computing and computer-assisted intervention - MICCAI2001*, volume 2208 of *Lecture Notes in Computer Science*, pages 204–212, October 2001.
7. Lucien Nocera and James C. Gee. Robust partial volume tissue classification of cerebral MRI scans. In K. M. Hanson, editor, *SPIE Medical Imaging*, volume 3034, pages 312–322, February 1997.
8. Aljaž Noe, Stanislav Kovačič, and James C. Gee. Segmentation of Cerebral MRI Scans Using a Partial Volume Model, Shading Correction, and an Anatomical Prior. In *Proceedings of the SPIE Symposium on Medical Imaging 2001: Image Processing*, volume 4322, pages 1466–1477, San Diego, California, USA, February 2001.
9. David W. Shattuck, Stephanie R. Sandor-Leahy, Kirt A. Schaper, David A. Rottenberg, and Richard M. Leahy. Magnetic resonance image tissue classification using a partial volume model. *NeuroImage*, 13(5):856–876, May 2001.